Study of the performance of glucose anomers in a hydroxide anion exchange membrane electrolyzer operating with pulse electrodeposited gold for paired electrosynthesis

Zahra Hagheh Kavousi, Amira Ben Abderrahmane, Massomeh Ghorbanloo, Sophie Tingry, David Cornu, Mikhael Bechelany, Yaovi Holade

Study of the performance of glucose anomers in a hydroxide anion exchange membrane electrolyzer operating with pulse electrodeposited gold for paired electrosynthesis

Zahra Hagheh Kavousi,[a,b,+] Amira Ben Abderrahmane,[a,+] Massomeh Ghorbanloo,[b] Sophie Tingry,[a,c] David Cornu,[a,c] Mikhael Bechelany[a,d] and Yaovi Holade,[a,c,*]

[a] *Institut Européen des Membranes, IEM, UMR, 5635, Univ Montpellier, ENSCM, CNRS, 34090 Montpellier, France*

[b] *Department of Chemistry, Faculty of Sciences, University of Zanjan, P.O. Box: 4537138791, Zanjan, Iran*

[c] *French Research Network on Hydrogen (FRH2), Research Federation No. 2044 CNRS, BP 32229, Nantes CEDEX 3 44322, France.*

[d] *Gulf University for Science and Technology, GUST, Kuwait*

*Corresponding author: yaovi.holade@enscm.fr (Y.H.). ORCID: 0000-0002-8806-568X

[+]These authors contributed equally to this work.

ABSTRACT

Electroconversion (also known as electroreforming) of biomass-derived compounds is currently attracting considerable interest, with the aim of lowering cell voltage during electrolysis to co-produce a number of decarbonized energy carriers or chemical intermediates (hydrogen, ammonia, gluconate, etc.). Naturally, D-glucose, which represents a study model for the electro-valorization of cellulosic biomass into value-added chemicals such as gluconate, is in fact a mixture of two anomers called α-D- and β-D-glucose. The β-D-glucose anomer is the monomer unit of cellulose, while the α-D-glucose anomer is the monomer unit of starch. In this contribution, we therefore investigate whether or not the nature of the glucose substrate can influence electrolysis cell performance, or whether the use of D-glucose alone can represent the true picture of biomass feeding an electrolysis cell. Free-standing electrocatalysts ready for use in a membrane-electrode assembly were synthesized using a pulsed electrodeposition methodology to control the deposition of gold and platinum particles on the microfibers of a low-metal gas diffusion electrode (GDE). We developed GDE-Au (82 μg_{Au} cm^{-2}, 0.88 wt%) to catalyze the selective electrooxidation of glucose into gluconate, and GDE-Pt (33 μg_{Pt} cm^{-2}, 0.36 wt%) to catalyze the hydrogen evolution reaction (HER). While half-cell studies showed no significant difference, for the glucose-fed electrolysis cell, α-D-glucose leads to a much

higher current density compared to D-glucose and β-D-glucose for cell voltages above 0.5 V, leading to 85.6 ± 17.1, 44.3 ± 8.8 and 30.5 ± 0.8 mA cm^{-2} for α-D-glucose, β-D-glucose, and D-glucose, respectively, at 1 V.

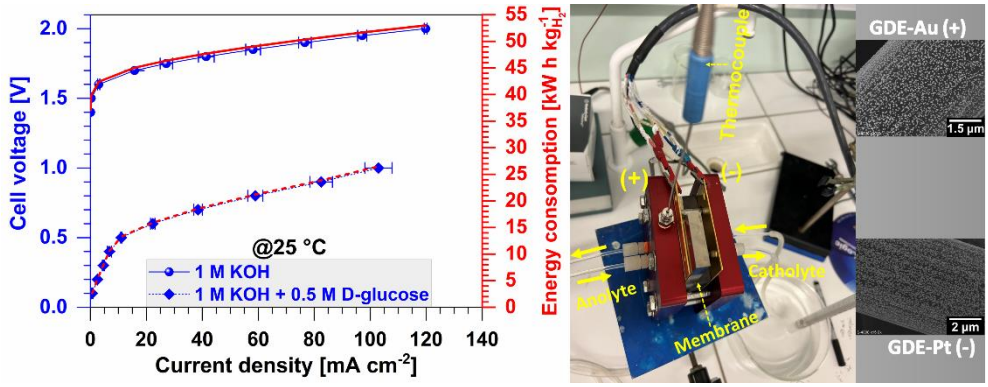

Keywords:

Glucose electrooxidation

Biomass electroconversion

Anion exchange membrane

Gas diffusion electrode

Electrodeposition

1. Introduction

Over the last ten years, the study of electrooxidation reactions of organic compounds has rapidly expanded, with the aim of discovering a low-energy anode for cathodic processes of societal and economic importance (H_2, ammonia, CO_2) [1-4]. In fact, the oxygen evolution reaction (OER, $2H_2O \rightarrow O_2 + 4H^+ + 4e^-$ or $4OH^- \rightarrow O_2 + 2H_2O + 4e^-$) cannot start before the potential of E = 1.23 V vs RHE (reversible hydrogen electrode), actually around 1.4 V vs RHE, which is significantly larger than the hydrogen evolution reaction (HER, $2H^+ + 2e^- \rightarrow H_2$ or $2H_2O + 4e^- \rightarrow H_2 + 2OH^-$), CO_2 reduction reaction (CO2RR) or N_2/nitrate reduction reaction (NRR) happening between -0.5 and 0 V vs RHE, which results into a high electricity demand [3,5-7]. Consequently, a large number of organic compounds such as methanol, ethanol, glycerol, glucose, 5-hydroxymethylfurfural (5-HMF), cellulose, lignin, polyethylene terephthalate (PET) plastic, etc. are being investigated as anode substrates due to their lower oxidation potential in comparison to OER, that is, E = 0-1 V vs RHE [1,2,8-17]. Biomass-derived compounds are receiving the most attention, as they are abundant and their selective electrooxidation could enable dual electrosynthesis at the anode and cathode, known as paired electrosynthesis in synthetic organic electrochemistry [18-21]. More specifically, the electrocatalytic conversion (also known as upgrading or electro-reforming) of biomass derivatives, where the anodic reaction of an electrolyzer, e.g. the OER, is replaced by the electro-oxidation of abundant biomass, provides the opportunity to reduce cell voltage and, at the same time, co-produce important renewable chemicals for the manufacture of biopolymers, detergents, food ingredients, etc. [21-24].

Glucose, which represents the cellulosic biomass, has therefore been the subject of numerous studies, devoted to the production of glucaric and/or gluconic acid [21,25-27]. We note that glucaric acid is one of the Top-12 constituents of high-value bio-based chemicals or materials, while gluconic acid is one of the Top-30 [28]. For example, although both have high commercial potential [25,27-31], the cost of electrical energy could be less than USD $40 per ton of gluconic acid (plus the co-production of 12-13 kg of high-purity H_2) through paired electrolysis, compared with biotechnological methods (USD $500-2000) which mainly account for the world's gluconic acid production of 100,000 tons per year [25]. Regarding the electrooxidation of organic compounds (coupled proton/electron steps), seminal studies have shown that the efficiency is peaked at a pH close to the compound's pKa, as the alkoxide (dissociated anion) could be an active species [32-37]. Consequently, since glucose as well as the other sub-units of the cellulose have a pKa of 11-13 [32-36], the alkaline medium was the

electrolyte, but we still lack insight into whether selectivity could be maintained at a higher current density (>0.1 A/cm^2) in an electrolyzer to maintain satisfactory H_2 productivity, for example. Indeed, the majority of studies are realized in an H-type electrochemical cell or do not reach a significant current density for reliable H_2 co-production [3,21,25]. For example, Verma *et al*. [3] observed that a flow CO_2 electrolysis cell electrolyzer (catholyte: 2 M KOH + CO_2; anolyte: 2 M KOH + 2 M substrate (glycerol or glucose)), leads to a partial CO current density of 12.5 and 88.4 mA cm^{-2} at a cell voltage of 1.5 V for glucose and glycerol, respectively. The relatively low diffusion coefficient of the glucose molecule (D = 6.9×10^{-10} cm^2 s^{-1}) [38] affects mass transport and glucose degradation at temperatures above 40 °C [39] actually limits the possibility of targeting a higher current density for such a cascade of multi-electronic and multi-proton reaction [33], which induce numerous reaction intermediates and higher overpotential energy barriers. Consequently, fundamental studies have been devoted to understanding the mechanism of selective glucose electrooxidation for better guidance in the engineering of gold-based electrocatalysts, which is the only material allowing a compromise between selectivity and electrode potential so as not to compete with OER. Leveraging differential electrochemical mass spectrometry (DEMS), Faverge *et al*. [26] recently observed the formation of H_2 during the electrocatalytic oxidation of glucose on Au in the potential range of 0.35-0.50 V vs RHE, attributed to the recombination of adsorbed protons (H_{ads}) resulting from glucose dehydrogenation. We note that the widely used D-glucose is a mixture of α-D and β-D (the different forms of glucose are shown in Fig. 1a), whereby the β-D-glucose anomer is the monomer unit of cellulose while the α-D-glucose anomer is the monomer unit of starch. This means that the use of D-glucose alone may not represent the true picture of biomass feeding an electrolysis cell (Fig. 1b), even though many hours waiting to reach equilibrium is common in bioelectrochemistry due to the prevailing opinion on the better reactivity of the β-D anomer [40-44]. Indeed, Fig.1b clearly shows that using glucose at the anode of an electrolyzer entails a much lower electricity consumption than a water-based system.

We have recently carried out a multivariate study with half-cell and potential-dependent energy profiles, calculated by density functional theory (DFT), to address the possible reactivity discrepancy between the three glucose forms: α-D, β-D and D [16]. The results established the better electrocatalytic reactivity of the α-anomer compared with the β-anomer at neutral pH and the reverse at alkaline pH on bare gold particles directly grown on a gas diffusion electrode to bypass organic surfactants that alter activity trends. An open question remains as to how these different forms of glucose behave in an electrolysis cell, whose performance may be

considerably different from that in a half-cell [45,46]. Hence, the scope of the present study is to interrogate the behavior of different glucose anomers in a hydroxide anion exchange membrane (Sustainion® X37-50 grade RT) based electrolysis cell. We leverage our switchable pulse electrodeposition methodology to prepare self-supported electrocatalysts on three-dimensional electrically conductive gas-diffusion electrode (GDE), using gold as a model at the anode so as not to break the carbon-carbon bond and to achieve cell voltages below 1-1.2 V.

2. Experimental details

2.1. Materials

Hexahydrate hexachloroplatinic(IV) acid ($H_2PtCl_6 \cdot 6H_2O$, 99%), trihydrate tetrachloroauric (III) acid ($HAuCl_4 \cdot 3H_2O$, 99.9%, Sigma-Aldrich), potassium hydroxide (KOH, 99.98% (trace metal basis), Acros Organics), potassium nitrate (KNO_3, Sigma-Aldrich, 99.0% min), D-(+)-glucose (BioXtra, ≥99.5% (GC), Sigma-Aldrich), α-D-(+)-glucose (99+%, Acros Organics: ordered from Fischer Scientific), β-D-glucose (97%, MP Biomedicals™: ordered from Fischer Scientific), lead (II) nitrate ($Pb(NO_3)_2$, ≥99.0%, Sigma-Aldrich), isopropanol (iPrOH, ≥99.5%, Sigma-Aldrich), potassium bromide (KBr, ACS, 99% min, Alfa Aesar), Fumion FAA-3-SOLUT-10 (FuMA-Tech, Fuel Cell Store), commercial Pt/C (20 wt%, 2 nm particles size, Premetek Co., USA), and commercial Au/C (20 wt%, ≈4 nm particles size, Premetek Co., USA) were used as-received. GDE-based carbon paper (GDE, AvCarb MGL190, 190 μm thickness) was obtained from Fuel Cell Earth LL (USA) and washed by iPrOH prior to use. Hydroxide anion exchange membrane (AEM, Sustainion® X37-50 grade RT, 50 μm dry thickness) was purchased from Fuel Cell Store (US) and activated in 1 M KOH for 24 h at room temperature (22 ± 3 °C) and copiously washed with Milli-Q water prior to use. Ar (grade 5.0) was purchased from Air Liquide, France. The used water was ultrapure with a resistivity of 18.2 MΩ cm at 20 °C and was provided by a Milli-Q Millipore source.

2.2. Synthesis of GDE-Au and GDE-Pt electrodes

We leverage our previous methodology [16] for galvanostatic electroshock growth of Au and Pt particles on GDE. Pieces of GDE (AvCarb MGL190, 190 μm thick, Fuel Cell Earth LL, USA) were cut into a T-shape (3 cm × 3 cm usable size and 1 cm × 1 cm on top for electrical wiring with gold (Alfer Aesar)) and washed with isopropanol (three cycles of 5 min each, orbital

shaker) and dried (50 °C, 1 h). Next, electroplating tape (3M Company) was applied on one side to control one-sided particle deposition. The synthesis was carried out in a single-compartment, three-electrode electrochemical cell consisting of a homemade double-shell glass cell with water circulation at 25 °C. The working, counter and reference electrodes were GDE, glassy carbon plate (Alfer Aesar, 23 cm^2) and silver-silver (Ag|AgCl|KCl (3 M), Radiometer; denoted as Ag/AgCl), respectively. Synthesis was performed under gentle agitation. Typically, 83.1 mL 0.1 M KNO_3, 16.9 mL stock solution (prepared in 0.1 M KNO_3) of 1.3 mM $HAuCl_4 \cdot 3H_2O$ (for GDE-Au) or 1.3 mM $H_2PtCl_6 \cdot 6H_2O$ (for GDE-Pt), and 31.4 mg KBr (n(KBr)/n($HAuCl_4$ or H_2PtCl_6) = 12) were added and outgassed with Ar for 15 min. The pulsed electrodeposition program was performed using a VSP-3e potentiostat, Biologic Science Instruments. The program consisted of an OFF step (open circuit potential (OCP) i.e. I_{OFF} = 0, τ_{OFF} = 5 s, relaxation), an ON step (I_{ON} = -2.7 mA, τ_{ON} = 5 s, deposition), and a repeat loop (N_{cycles} = 180). At the end of the deposition, the GDE-Au or GDE-Pt was rinsed several times with water and dried in an oven at 80 °C for 1 h to trigger the self-peeling of the 3M electroplating tape (drying temperature (40-80 °C) and duration (from a few minutes to a few hours) depend on the batch of 3M electroplating tape). Finally, the tape is carefully removed and the electrodes are ready for use.

2.3. Physico-chemical characterization

Scanning electron microscopy (SEM) was acquired on a Hitachi S-4800 microscope, while qualitative energy-dispersive X-ray (EDX) analysis was conducted on a ZEISS EVOHD 15 microscope. X-ray diffraction (XRD) analysis was undertaken in Bragg-Brentano mode 2θ = 35-85°) on a Bruker D8 Discover diffractometer operating with $Cu_{K\alpha1}$ radiation at a wavelength of 1.5406 Å (40 kV, and 40 mA). Elemental analysis was made using inductively coupled plasma optical emission spectrometry (ICP-OES, Agilent 5110 VDV).

2.4. Electrochemical Measurement

The half-cell study was carried out in a single-compartment, three-electrode electrochemical cell, consisting of a home-made double-shell glass cell with water circulation at 25°C, using a VSP-3e potentiostat, Biologic Science Instruments. The working electrode was made by cutting the parent electrode, GDE-Au or GDE-Pt, into an L-shape of 1 cm × 1 cm usable size and 0.3 cm × 1 cm on top for electrical wiring with gold. The counter and reference electrodes were

glassy carbon (6 cm^2) and a reversible hydrogen electrode (RHE, HydroFlex® Hydrogen Reference Electrode, Biologic) respectively. The electrolyte was 1 M KOH. Lead underpotential deposition (Pb_{UPD}) was carried out in 1 M KOH + 1 mM $Pb(NO_3)_2$. The electrooxidation reaction of glucose (0.1 M; different forms of D-, α-D- and β-D-glucose) and HERs were studied using cyclic voltammetry (CV), linear scanning voltammetry (LSV) and potentiostatic electrochemical impedance spectroscopy (EIS, 100 kHz to 100 mHz, 10 mV amplitude, 10 points per decade, unstirred solution at different electrode potentials (see text)). Unless otherwise indicated, voltammograms reported and potentials applied during EIS were not corrected by the iR-drop (ohmic resistance of 2.0-2.4 Ω for the above electrode sizes of synthesized GDE-based electrocatalysts). To test the commercial catalyst (20 wt% Au/C and 20 wt% Pt/C), catalytic inks were prepared by ultrasonically mixing (ice bath, Elmasonic sonication bath (Grosseron, France)): (i) 400 µL MQ water + 400 µL of iPrOH + catalyst (16.0 mg of Au/C or 6.6 mg of Pt/C) for 15 min, and (ii) the previous mixture plus Fumion (13.0 mg for Au/C and 5.3 mg for Pt/C) for 10 min. We note, to get a high-quality catalytic ink while minimizing the supported catalysts degradation, the duration depends on many parameters (catalyst, solvent, sonication system, ionomer, etc.) [47-49]. After reaching the desired ink homogeneous, a suitable volume was drop-casted onto each face of a bare L-shape GDE of similar size (above) and dried at room temperature to reach a loading of 82 $\mu g_{Au}\ cm^{-2}$ (for Au/C) and 33 $\mu g_{Pt}\ cm^{-2}$ (for Pt/C), which are the range of the loadings found for our synthesized electrocatalysts for a fair comparison of the performance.

For the full-cell, that is, hydroxide anion exchanged membrane electrolysis, the experiments were performed using the Scribner's "Dual Area Fixture" (5 and 25 cm^2 active area; herein, we used 5 cm^2 pattern). SP-150 potentiostat (Biologic Science Instruments), controlled by the EC-lab software, was used to conduct the electrochemical measurements. The anolyte (100 mL min^{-1}) and catholyte (150 mL min^{-1}) were recirculated between the electrochemical cell and the storage tanks with peristaltic pumps (Hei-FLOW Ultimate 600, Heidolph, Germany; and BT100L, Lead Fluid, China).

3. Results and discussion

3.1. Synthesis of GDE-Au and GDE-Pt electrodes

To control the metal loading on GDE, necessary for membrane-electrode-assembly (MEA) to manage mass transport and achieve higher current densities [50], we developed a pulse electrodeposition approach, also known as electroshock synthesis [15,16,51-54]. Fig 2a shows

the program for the designed galvanostatic configuration that rapidly switches the applied current bias to overcome any reduction and mass transport kinetics in the vicinity of the electrode and trigger the formation of relatively uniform particles on the GDEs. We implemented this strategy to avoid any catalytic ink preparation steps that might impact on the reliability of the comparison between different glucose anomers. The galvanostatic electroshock program consists of a relaxation step to renew the double layer [open circuit potential (OCP); I_{OFF} = 0, τ_{OFF} = 5 s] and a metal salt reduction step (I_{ON} = -2.7 mA, τ_{ON} = 5 s, deposition] for a GDE size of 3 cm × 3 cm (one side masked), that is, a current density of j = -0.3 mA cm^{-2} (not taking into account the 3D structure of GDE). These two sequences are repeated until a total duration of 30 min is reached. As per our previous study, this represents a compromise in terms of particle size and total metal content, while striking a balance between metal salt reduction and the parallel HER. Bromide anions were used to regulate the nucleation and growth of metal seeds into bare, monodisperse particles without any organic surfactants that might compromise the electrocatalytic activity of the synthesized electrocatalyst [55,56].

The difference in amplitude during applied bias is attributed to the difference in reduction kinetics of $AuBr_4^-$/Au ($E°(AuBr_4^-/Au)$ = 0.8 V vs Ag/AgCl) compared to $PtBr_6^{2-}$/Pt ($E°(PtBr_6^{2-}/Pt)$ = 0.5 V vs Ag/AgCl) [57,58]. Fig. 2b is a representative SEM image of the synthesized GDE-Au electrode, showing the electrolyte level during synthesis and thus the limit of metal deposition. To validate the hypothesis of a low metal loading, we performed element analysis by ICP-OES. The results are gathered in Table 2. The metal loading relative to the entire electrode is well below 1 wt%, that is, 82 and 33 μg_{metal} cm^{-2} when considering only the external geometric area of the GDE that was facing the electrolyte. Later on, it will be shown that only the first 2-3 layers of microfibers are decorated by particles.

3.2. Physicochemical characterization of GDE-Au and GDE-Pt electrodes

We next used X-ray diffraction (XRD) to assess the crystallinity of the synthesized free-standing electrodes. Fig. 1c shows that a predominant carbon diffraction peak at 54.7° from graphite (004), already present in the pristine GDE material, is also visible in the diffractogram of GDE-Au and GDE-Pt materials. For the latter, the main diffraction peaks at 38.3° and 40.1° correspond to the (111) crystallographic orientations of the face-centered cubic (cfc) structure of gold and platinum, respectively. The crystallite size and lattice parameter evaluated by the Debye-Scherrer equation and Bragg's law [59-62] and compiled in Table 1 are consistent with gold and platinum and with the expected particle size of less than 80 nm. A much smaller particle size could be achieved by adjusting the pulse electrodeposition conditions, as

previously demonstrated [16]. Furthermore, the EDX spectrum in Fig. 2d shows that the only species are either carbon and gold for GDE-Au, or carbon and platinum for GDE-Pt, confirming that the KBr used to regulate electrodeposition kinetics has been well removed (previous analysis by X-ray photoelectron spectroscopy (XPS) revealed no additional contaminant [16,56]). We note that the ubiquitous presence of oxygen in Fig. 2d and in the EDX maps of Figs. 2e-f results from the SEM sample holder used and/or the natural passivation of metal species when exposed to ambient air. Furthermore, the element mapping in Figs. 2e-f confirms the homogeneous distribution of metal particles, which can be confirmed by the SEM images in Figs. 3a1-3b8 for GDE-Pt and Figs. 3b1-3b8 on the electrode surface. It should be emphasized that the high intensity dots in Figs. 2-f that might suggest particle agglomerates are in fact due to the initial structure of the GDE, as shown in Fig. 3b6 (a zoom of a section of Fig. 3b5). Depending on the location of the initial GDE support (isolated fibers, intersection of several fibers, several fibers bonded together, etc.), surface defects have an impact on particle growth, resulting in size anisotropy, but the extent of size anisotropy remains below 80 nm. Interestingly, closer examination of the micrographs reveals that particles are deposited only on the first 2-3 layers of microfibers, out of around 30 layers (given a thickness of 190 µm and an average fiber diameter of 7 µm). Moreover, particle size decreases from the outer to the inner microfibers, even though the electrode was initially well wetted by the electroplating solution. As the outer microfibers are much closer to the counter-electrode, they are subjected to a high applied electric field between the working electrode and the counter-electrode, resulting in preferential nucleation and growth on the outer microfibers. This establishes not only a concentration gradient for the metal precursor, but also a shielding effect that could also promote diffusion of the metal precursor towards the surface where the first seeds are formed [15,56]. Alongside the electrochemical reduction kinetics of $AuBr_4^-$/Au ($E°(AuBr_4^-/Au)$ = 0.8 V vs Ag/AgCl) versus $PtBr_6^{2-}$/Pt ($E°(PtBr_6^{2-}/Pt)$ = 0.5 V vs Ag/AgCl), the low metal charge and small particle size for the GDE-Pt electrode compared with GDE-Au may be explained by the superior kinetics of Pt for HER compared with Au. Indeed, the first deposited particles are likely to catalyze HER where, moreover, the rapid generation and dissipation of H_2 bubbles partially inhibits the coalescence and the fusion of seeds into bigger particles [51-54].

3.3. Half-cell electrochemical characterization of GDE-Au and GDE-Pt electrodes

Having demonstrated, by XRD and SEM, the ability of the galvanostatic electroshock approach to control ON and OFF current switching to form relatively small and uniform Au and Pt particles, we then used cyclic voltammetry (CV) to electrochemically probe the different

electrodes in a 1 M KOH electrolyte (Fig. 4a). The CV profiles of GDE-Pt and GDE-Au are characteristic of Pt and Au materials in an alkaline electrolyte, respectively. For GDE-Pt, faradaic processes between 0.05 and 0.45 V vs RHE are associated with adsorption and desorption of protons from Pt sites ($Pt + H_2O + e^- = Pt\text{-}H + OH^-$), which are followed by the double layer up to 0.7 V vs. RHE and finally by platinum oxide formation and reduction at higher potentials. The specific electrochemically active surface area of the proton desorption region, using a monolayer charge of Q_H = 210 μC cm^{-2}, was 97 m^2 g^{-1}, which is higher than the value obtained for commercial Pt/C (21 m^2 g^{-1}). We note that Pt/C catalytic ink was drop-cast onto each face of an L-shaped bare GDE of similar size to the GDE-Pt tested to achieve the same 33 μg_{Pt} cm^{-2} loading as for our synthesized electrocatalyst for a fair comparison of performance. For GDE-Au, which is known not to exhibit proton adsorption and desorption regions (weak interaction [63]), the main processes are the double layer – whose capacity changes with increasing potential due to water and hydroxyl adsorption – and the formation and reduction of gold oxide at high potentials. The specific electrochemically active surface area resulting from the reduction of these oxides, using a monolayer loading of Q_{AuOx} = 400 μC cm^{-2} for an upper potential limit of 1.55 V vs RHE [64] (an upper potential limit of 1.6 V vs RHE leads to Q_{AuOx} of ca. 480 μC cm^{-2} [65,66]), was 8 m^2 g^{-1}, which is similar to the value obtained for the commercial Au/C (7 m^2 g^{-1}). Additionally, the CV at different scan speeds in Fig. 4b corroborates the reversibility of Pb_{UPD} limited by the adsorption and stripping of lead from the gold surface consisting of (111) and (110) facets [56,66-69].

Before integrating the two electrodes into the electrolysis cell (GDE-Pt as cathode and GDE-Au as anode), we first interrogated performance in half-cell. Fig. 4c shows the LSV of HER for the synthesized GDE-Pt and the commercial Pt/C (same loading of 33 μg_{Pt} cm^{-2}). The higher electrochemically active surface area of GDE-Pt translates into better electrocatalytic kinetics with an overpotential around 40 mV lower than Pt/C. However, as SEM images of GDE-Pt show, Pt is only deposited on the first 3 microfiber layers, whereas in the case of Pt/C, all microfiber layers (around 30) are expected to contain Pt. Normalization by the number of microfiber layers actually containing Pt particles thus gives a substantial increase in activity that can reasonably be attributed to the synthesis method, since direct contact of the Pt with the GDE support accelerates electron transfer kinetics.

The results of the electrocatalytic glucose oxidation reaction are shown in Figs. 4d-e (voltammograms) and in Figs. 4f-i (EIS). Here, leveraging previous studies with bulk structures and nanostructures at different pHs [16,70], an alkaline electrolyte was used to achieve high current density during electrolysis in order to target significant H_2 co-production rate in the

current context of low-energy glucose-fueled electrolyzers [3,21-25,71-78]. Quantitative data from the fitting of the Nyquist impedance plots in Figs. 4g-4i for modeling the electrocatalytic interface by EIS are reported in Table 2. The equivalent electrochemical circuit (EEC) was $R_{\Omega}+Q_{CPE}//R_{ct}$ where R_{Ω} is naturally the total ohmic resistances (cell resistance), R_{ct} is the reduced charge transfer resistance, and Q_{CPE} is the capacitance of the constant phase element [79,80]. The current density as well as the charge transfer resistance follow the same order. Although SEM images of GDE-Au show that Au is deposited only on the first 3 microfiber layers, whereas for Au/C all microfiber layers (approx. 30) are expected to receive Au during catalytic ink coating, the current density in Fig. 4d is similar up to 0.8 V vs. RHE. Fig 4e, which shows the normalization of current by the number of microfiber layers actually containing Au particles, highlights a higher "activity" that can logically be attributed to the direct contact of Au with the GDE support. For comparison with relevant nanocatalysts, the geometric current density (for example, for drawing high production rate of H_2 in electrolyzers), the as-synthesized GDE-Au with 82 μg_{Au} cm^{-2}, without any organic surfactant on the particle surface and benefiting from a strong particle-support interaction, is higher than most of the literature where the metal is even hundreds of micrograms per square centimeter [25,81-85].

The Tafel slope of 118-134 mV dec^{-1} (Fig. 4f) suggests that the reaction is limited by glucose dehydrogenation, the so-called Volmer reaction [86]. We note that the theoretical value of 118-120 mV dec^{-1} is expected for a symmetry coefficient of $\alpha = 0.5$, however, according to asymmetric Marcus theory, this parameter can deviate from the value of 0.5 if the reactant exchanges an electron with the metal while in the adsorbed state and induces the reorganization of the medium required to reach the transition state [87,88]. It is worth mentioning that the Tafel slope describes the reaction mechanism [89,90] in contrast to many misunderstandings and assertions in the literature that use the Tafel slope as an explicit measure of electrocatalytic activity, i.e., which electrocatalyst is superior to the other.

3.4. Hydroxide anion exchange membrane based glucose electrolyzer

Having characterized the electrodes and validated their electrochemical behavior through half-cell studies, we finally evaluated performance in an electrolysis cell, the schematic diagram of which is shown in Fig. 5a. We reiterate that the ultimate aim of this work is to investigate whether or not the nature of the glucose substrate can influence the performance of the electrolysis cell, which, to our knowledge, has not yet been done. Indeed, D-glucose, which represents a model for the study in the existing literature of abundant cellulosic biomass, can exist in two forms: the anomeric β-D-glucose, which is the monomeric unit of cellulose, and

the anomeric α-D-glucose, which is the monomeric unit of starch. And so, the D-glucose widely used in the literature is actually a mixture of α-D and β-D (see Fig. 1a). We specifically seek to elucidate whether or not the use of D-glucose represents the true picture of biomass feeding an electrolysis cell. The cathode (GDE-Pt) and anode (GDE-Au) were pressed together with a hydroxide anion exchange membrane (AEM, Sustainion® X37-50 grade RT, 50 μm dry thickness). The GDE-Au anode was chosen as a model electrocatalyst to represent selective electroconversion without breaking C-C carbon bonds, which we recently demonstrated by performing bulk electrolysis under different configurations of fixed currents or electrode potentials [16]. Here, we validated the complete cell by analyzing the anolyte by chromatography to ensure that gluconate is still the main oxidation product for all three glucose types: D-, α-D and β-D-glucose (see Fig. 1a). Furthermore, electrolysis experiments were carried out at 25 °C to avoid possible glucose decomposition [39], while the investigative methods were EIS (Fig. 5b-c) and polarization curves by the potentiostatic method (0.05 V step, Fig. 5d) and LSV method (0.05 V s^{-1} scan rate, Fig. 5e).

Furthermore, to conclusively attribute the two depressed semicircles in the Nyquist impedance plots to cathode and anode processes, we varied the cell voltage in the absence and presence of glucose. In conventional water electrolysis, the depressed semicircle at high frequency (low values of Z') is generally associated with HER featuring much faster kinetics than OER [79,80,91-94], which is intuitively correct and confirmed by Fig. 5d when cell voltage is increased from 1.5 to 1.7 V. Fig. 4c, whose results from fitting by the equivalent electrochemical circuit (EEC) of R_{Ω}+Q_{CPE}//$R_{ct\text{-}a}$+Q_{CPE}//$R_{ct\text{-}c}$) are presented in Table 3, clearly shows that the change in glucose concentration (0, 0.1 and 0.5 M) only affects the low-frequency part of the circuit (high values of Z'), and therefore concerns the anode, since the cathode remains unchanged. Increasing the D-glucose concentration from 0.1 to 0.5 M is logically accompanied by an increase in current density, regardless of the method used to record the polarization curves (Fig. 5d vs Fig. 5e). The photos of the anolyte before and after electrolysis highlights the yellowing of the solution, which becomes more intense with increasing glucose or electrolyte content. Although the difference in color before and after electrolysis can logically be explained by the increased conversion rate (the yellow color is due to gluconate) considering the current densities (Figs. 5d-5e), the other factor is the chemical stability of glucose in basic media, where nucleophilic attack of OH^- on the anomeric carbon is possible, accelerated in non-degassed solution. We observed the increase in yellow color when 1 M KOH + 0.5 M D-glucose were left for several hours. While the small variation in ohmic resistance for 0 and 0.1 M D-glucose (R_{Ω} = 190-200 mΩ cm^2) is within the experimental range,

we note that R_Ω increases substantially from 190 to 230 mΩ cm^2 (Table 3) when the concentration of D-glucose increases from 0.1 to 0.5 M. Such variation is attributed to the increased viscosity of the anolyte, since the other components of the ensemble remain unchanged. However, we do not rule out a slight deviation arising from discrepancies in contact with the current collector or assembly issues during the MEA process.

Analysis of Figs. 5d-5e shows that the dynamic method can lead to an overestimation of performance, not least because it is very difficult to achieve a quasi-stationary regime even with slow rates of 0.005-0.001 V s^{-1}. On the other hand, for the potentiostatic method described here (the galvanostatic method is also possible, but has not been tested here), staying on voltage levels for prolonged periods can accelerate poisoning of active sites due to the accumulation of intermediates and reaction products. It would therefore be necessary to find a way of comparing the various results in the literature. In the present exploratory study, we have chosen not to privilege one method and thus allow the whole community to exploit our results. In the half-cell studies, pulsed electrolysis, similar to the strategy adopted for electrocatalyst synthesis, is used, since the aim is not to target H_2. Such a strategy could perhaps allow a compromise between stability and the co-produced amount of H_2.

Regarding energy consumption, the ordinate axis on the right in Figs. 5d-5e logically confirms that the energy required to produce 1 kg H_2 is at least halved when the anode is supplied with D-glucose, as predicted by the thermodynamics in Fig. 1b. However, the current density remains too low if substantial H_2 productivities are targeted, that is, j = 0.2-2 A cm^{-2} [5]. Still, for applications where large quantities of H_2 are not required and access to electricity is complicated, the anode can be supplied with D-glucose. As the cell voltage remains below 1 V, taking into account the half-cell results in Figs. 4c-4d, we can assume that the anode potential does not exceed 0.4-0.7 V vs. the HRE. This minimizes anode corrosion phenomena, which could contribute to the overall cost of electrolysis cell assembly.

Based on the above observations, a concentration of 0.1 M in glucose was used to study the electrolysis performance of the different forms of glucose (D-, α-D-, and β-D-glucose). Figs. 6a-6c show the results obtained in terms of polarization curves and EIS (quantitative data in Table 4). Table 5 compares performance with existing literature. Electrolysis starts at a cell voltage as low as 0.1 V, which is significantly low compared with the existing literature on low-energy glucose-fed electrolyzers [3,21,25,71-78]. While half-cell polarization curves and EIS analysis revealed no significant difference, full-cell tests reveal that, whatever the performance evaluation method, a much higher current density can be achieved with α-D-glucose compared

to D-glucose and β-D-glucose. Specifically, at a cell voltage of 1 V, Fig. 6b shows that the current density is 44.3 ± 8.8 mA cm^{-2} (D-glucose), 85.6 ± 17.1 mA cm^{-2} (α-D-glucose), and 30.5 ± 0.8 mA cm^{-2} (β-D-glucose). EIS data at a cell voltage of 0.6 V, Fig. 6c, were fitted with the EEC of R_{Ω}+Q_{CPE}//$R_{ct\text{-}a}$+Q_{CPE}//$R_{ct\text{-}c}$ depicting a electrolytic cell [79,80,91-94]. As we have seen previously, the depressed semicircle in the low-frequency region (high values of Z') is characteristic of the electrocatalytic process at the anode, since the change of anolyte only impacts this region (quantitative data in Table 4). The trend in charge transfer resistance of the anodic reaction ($R_{ct\text{-}a}$) is 12.43, 23.77, and 29.32 Ω cm^2 for α-D-glucose, D-glucose, and β-D-glucose, respectively, which is in agreement with the polarization curves. These results could be explained by the three-dimensional structure of the glucose molecule (Fig. 1a), whose impact on electrocatalytic activity becomes significant in the electrolysis configuration, where zero-gap assembly induces further phenomena of mass transport kinetics and interaction with active sites. The representative post-mortem SEM of Figs. 6d-g showed no significant particle damage on the microfibers.

4. Conclusion

In summary, for the first time to our knowledge, this study examined the potential impact of glucose type (α-D, β-D and D) on the performance of hydroxyl anion exchange membrane electrolysis (AEM, Sustainion® X37-50 grade RT). Indeed, D-glucose, which represents a model for the study of electroconversion (or electroreforming) of abundant biomass is in fact a mixture of α-D and β-D, the β-D-glucose anomer being the monomer unit of cellulose while the α-D-glucose anomer is the monomer unit of starch. Therefore, before considering the use of cellulosic biomass (a glucose polymer), it is necessary to understand the behavior of the different anomers in a representative electrochemical system other than the basic half-cell to envisage real applications. We therefore used pulsed electrodeposition to grow directly on the gas diffusion electrode, a small amount of gold particles (GDE-Au, 82 μg_{Au} cm^{-2}, 0.88 wt%) to catalyze the electrooxidation of glucose, and platinum particles (GDE-Pt, 33 μg_{Pt} cm^{-2}, 0.36 wt%) to catalyze the hydrogen evolution reaction (HER). The various electrodes were extensively characterized by physicochemical and electrochemical methods (SEM, EDX, XRD, ICP-OES, CV, LSV, EIS). In a half-cell, compared with Pt/C, GDE-Pt has a higher electrochemically active specific surface area (97 m^2 g^{-1} vs 21 m^2 g^{-1}) and HER activity (40 mV lower overpotential). For GDE-Au, the specific electrochemically active surface area (8 m^2 g^{-1}) is comparable to commercial Au/C (7 m^2 g^{-1}) and the same trends was observed for glucose

electrooxidation. The glucose-fed electrolysis cell starts at a voltage as low as 0.1 V and showed that α-D-glucose leads to a much higher current density in comparison with D-glucose and β-D-glucose for cell voltages above 0.5 V. For a voltage of 1 V, the current density recorded for polarization curves recorded at 0.05 V s^{-1} is 85.6 ± 17.1, 44.3 ± 8.8 and 30.5 ± 0.8 mA cm^{-2} for α-D-glucose, β-D-glucose, and D-glucose, respectively. The origin of such a discrepancy is not yet clearly known, but we hypothesized that the impact of the three-dimensional structure of the glucose molecule on electrocatalytic activity becomes significant in the zero-gap assembly, which could induce other phenomena of material transport kinetics and interaction with active sites, as is well known in the classical situation of water electrolysis. As far as energy consumption is concerned, our results confirm that the energy required to produce 1 kg H_2 can be easily divided by at least 2 compared with conventional water electrolysis when the anode compartment is supplied with glucose substrate, even at current densities of 0.10-0.15 A cm^{-2}, which may be suitable for applications where large quantities of H_2 are not required and/or access to electricity is complicated. Although further studies are still needed, the present results provide a fundamental insight into the potential coupling of selective electroconversion of cellulosic biomass with cathodic reactions (HER, NRR, CO2RR, etc.) for the paired electrosynthesis of valuable chemicals and fuels with low energy input.

Declaration of competing interest

The authors declare that they have no known competing financial interests or personal relationships that could have appeared to influence the work reported in this paper.

Acknowledgments.

This work is financially supported by the French National Research Agency through the project MASTERS (ANR-22-CE43-0004), Chimie Balard Cirimat Carnot institute through the ANR program N°16 CARN 0008-01 (project REMEC, 19S08R06-FPV-HOLADE), LabEx CheMISyst (ANR-10-LABX-0501), and Montpellier University of Excellence I-SITE (project NANOGATE).

References

[1] F.W.S. Lucas, R.G. Grim, S.A. Tacey, C.A. Downes, J. Hasse, A.M. Roman, C.A. Farberow, J.A. Schaidle, A. Holewinski, Electrochemical Routes for the Valorization of Biomass-Derived Feedstocks: From Chemistry to Application, ACS Energy Lett., 6 (2021) 1205-1270.
[2] A. Caravaca, A. de Lucas-Consuegra, A.B. Calcerrada, J. Lobato, J.L. Valverde, F. Dorado, From biomass to pure hydrogen: Electrochemical reforming of bio-ethanol in a PEM electrolyser, Appl. Catal. B: Env., 134-135 (2013) 302-309.
[3] S. Verma, S. Lu, P.J.A. Kenis, Co-electrolysis of CO2 and glycerol as a pathway to carbon chemicals with improved technoeconomics due to low electricity consumption, Nat. Energy, 4 (2019) 466-474.
[4] R.L. Germscheidt, D.E.B. Moreira, R.G. Yoshimura, N.P. Gasbarro, E. Datti, P.L. dos Santos, J.A. Bonacin, Hydrogen Environmental Benefits Depend on the Way of Production: An Overview of the Main Processes Production and Challenges by 2050, Adv. Energy Sustainability Res., 2 (2021) 2100093.
[5] M. Chatenet, B.G. Pollet, D.R. Dekel, F. Dionigi, J. Deseure, P. Millet, R.D. Braatz, M.Z. Bazant, M. Eikerling, I. Staffell, Water electrolysis: from textbook knowledge to the latest scientific strategies and industrial developments, Chem. Soc. Rev., 51 (2022) 4583-4762.
[6] M. Wang, M.A. Khan, I. Mohsin, J. Wicks, A.H. Ip, K.Z. Sumon, C.-T. Dinh, E.H. Sargent, I.D. Gates, M.G. Kibria, Can sustainable ammonia synthesis pathways compete with fossil-fuel based Haber–Bosch processes?, Energy Environ. Sci., 14 (2021) 2535-2548.
[7] P.D. Luna, C. Hahn, D. Higgins, S.A. Jaffer, T.F. Jaramillo, E.H. Sargent, What would it take for renewably powered electrosynthesis to displace petrochemical processes?, Science, 364 (2019) eaav3506.
[8] T. Wang, L. Tao, X. Zhu, C. Chen, W. Chen, S. Du, Y. Zhou, B. Zhou, D. Wang, C. Xie, P. Long, W. Li, Y. Wang, R. Chen, Y. Zou, X.-Z. Fu, Y. Li, X. Duan, S. Wang, Combined anodic and cathodic hydrogen production from aldehyde oxidation and hydrogen evolution reaction, Nat. Catal., 5 (2022) 66-73.
[9] Y. Kwon, K.J.P. Schouten, J.C. van der Waal, E. de Jong, M.T.M. Koper, Electrocatalytic Conversion of Furanic Compounds, ACS Catal., 6 (2016) 6704-6717.
[10] J. White, L. Peters, D. Martín-Yerga, I. Terekhina, A. Anil, H. Lundberg, M. Johnsson, G. Salazar-Alvarez, G. Henriksson, A. Cornell, Glycerol Electrooxidation at Industrially Relevant Current Densities Using Electrodeposited PdNi/Nifoam Catalysts in Aerated Alkaline Media, J. Electrochem. Soc., 170 (2023) 086504.
[11] H. Zhang, Y. Wang, X. Li, K. Deng, H. Yu, Y. Xu, H. Wang, Z. Wang, L. Wang, Electrocatalytic upcycling of polyethylene terephthalate plastic to formic acid coupled with energy-saving hydrogen production over hierarchical Pd-doped NiTe nanoarrays, Appl. Catal. B: Env., 340 (2024) 123236.
[12] B. Guenot, M. Cretin, C. Lamy, Electrochemical reforming of dimethoxymethane in a Proton Exchange Membrane Electrolysis Cell: A way to generate clean hydrogen for low temperature fuel cells, Int. J. Hydrogen Energy, 42 (2017) 28128-28139.
[13] B. Guenot, M. Cretin, C. Lamy, Clean hydrogen generation from the electrocatalytic oxidation of methanol inside a proton exchange membrane electrolysis cell (PEMEC): effect of methanol concentration and working temperature, J. Appl. Electrochem., 45 (2015) 973-981.
[14] C. Lamy, T. Jaubert, S. Baranton, C. Coutanceau, Clean hydrogen generation through the electrocatalytic oxidation of ethanol in a Proton Exchange Membrane Electrolysis Cell (PEMEC): Effect of the nature and structure of the catalytic anode, J. Power Sources, 245 (2014) 927-936.
[15] R. Boukil, N. Tuleushova, D. Cot, B. Rebiere, V. Bonniol, J. Cambedouzou, S. Tingry, D. Cornu, Y. Holade, Enhanced electrocatalytic activity and selectivity of glycerol oxidation

triggered by nanoalloyed silver–gold nanocages directly grown on gas diffusion electrodes, J. Mater. Chem. A, 8 (2020) 8848-8856.
[16] Y. Holade, H. Guesmi, J.-S. Filhol, Q. Wang, T. Pham, J. Rabah, E. Maisonhaute, V. Bonniol, K. Servat, S. Tingry, D. Cornu, K.B. Kokoh, T.W. Napporn, S.D. Minteer, Deciphering the Electrocatalytic Reactivity of Glucose Anomers at Bare Gold Electrocatalysts for Biomass-Fueled Electrosynthesis, ACS Catal., 12 (2022) 12563-12571.
[17] Y. Holade, K. Servat, T.W. Napporn, C. Morais, J.-M. Berjeaud, K.B. Kokoh, Highly Selective Oxidation of Carbohydrates in an Efficient Electrochemical Energy Converter: Cogenerating Organic Electrosynthesis, ChemSusChem, 9 (2016) 252-263.
[18] C. Kingston, M.D. Palkowitz, Y. Takahira, J.C. Vantourout, B.K. Peters, Y. Kawamata, P.S. Baran, A Survival Guide for the "Electro-curious", Acc. Chem. Res., 53 (2020) 72-83.
[19] G. Hilt, Recent advances in paired electrolysis and their application in organic electrosynthesis, Curr. Opin. Electrochim, 43 (2024) 101425.
[20] H. Sheng, A.N. Janes, R.D. Ross, H. Hofstetter, K. Lee, J.R. Schmidt, S. Jin, Linear paired electrochemical valorization of glycerol enabled by the electro-Fenton process using a stable NiSe2 cathode, Nat. Catal., 5 (2022) 716-725.
[21] W.-J. Liu, Z. Xu, D. Zhao, X.-Q. Pan, H.-C. Li, X. Hu, Z.-Y. Fan, W.-K. Wang, G.-H. Zhao, S. Jin, G.W. Huber, H.-Q. Yu, Efficient electrochemical production of glucaric acid and H2 via glucose electrolysis, Nat. Commun., 11 (2020) 265.
[22] Y. Holade, N. Tuleushova, S. Tingry, K. Servat, T.W. Napporn, H. Guesmi, D. Cornu, K.B. Kokoh, Recent advances in the electrooxidation of biomass-based organic molecules for energy, chemicals and hydrogen production, Catal. Sci. Technol., 10 (2020) 3071-3112.
[23] M.A. Khan, T.A. Al-Attas, N.G. Yasri, H. Zhao, S. Larter, J. Hu, M.G. Kibria, Techno-economic analysis of a solar-powered biomass electrolysis pathway for coproduction of hydrogen and value-added chemicals, Sustainable Energy Fuels, 4 (2020) 5568-5577.
[24] T. Lepage, M. Kammoun, Q. Schmetz, A. Richel, Biomass-to-hydrogen: A review of main routes production, processes evaluation and techno-economical assessment, Biomass Bioenergy, 144 (2021) 105920.
[25] T. Rafaïdeen, S. Baranton, C. Coutanceau, Highly efficient and selective electrooxidation of glucose and xylose in alkaline medium at carbon supported alloyed PdAu nanocatalysts, Appl. Catal. B: Env., 243 (2019) 641-656.
[26] T. Faverge, B. Gilles, A. Bonnefont, F. Maillard, C. Coutanceau, M. Chatenet, In Situ Investigation of D-Glucose Oxidation into Value-Added Products on Au, Pt, and Pd under Alkaline Conditions: A Comparative Study, ACS Catal., 13 (2023) 2657-2669.
[27] M. Varničić, T. Vidaković-Koch, K. Sundmacher, Gluconic Acid Synthesis in an Electroenzymatic Reactor, Electrochim. Acta, 174 (2015) 480-487.
[28] T. Werpy, G. Petersen, Top value added chemicals from biomass: volume I--results of screening for potential candidates from sugars and synthesis gas, Pacific Northwest National Laboratory (PNNL), National Renewable Energy Laboratory (NREL), U.S. Department of Energy, Oak Ridge, TN, 2004.
[29] P. Pal, R. Kumar, S. Banerjee, Manufacture of gluconic acid: A review towards process intensification for green production, Chemical Engineering and Processing: Process Intensification, 104 (2016) 160-171.
[30] O.V. Singh, R. Kumar, Biotechnological production of gluconic acid: future implications, Appl. Microbiol. Biotechnol., 75 (2007) 713-722.
[31] S. Ramachandran, P. Fontanille, A. Pandey, C. Larroche, Gluconic acid: properties, applications and microbial production, Food Technol. Biotechnol., 44 (2006) 185-195.
[32] S.C.S. Lai, S.E.F. Kleijn, F.T.Z. Öztürk, V.C. van Rees Vellinga, J. Koning, P. Rodriguez, M.T.M. Koper, Effects of electrolyte pH and composition on the ethanol electro-oxidation reaction, Catal. Today, 154 (2010) 92-104.

[33] M.T.M. Koper, Theory of multiple proton-electron transfer reactions and its implications for electrocatalysis, Chem. Sci., 4 (2013) 2710-2723.
[34] J. Joo, T. Uchida, A. Cuesta, M.T.M. Koper, M. Osawa, Importance of Acid–Base Equilibrium in Electrocatalytic Oxidation of Formic Acid on Platinum, J. Am. Chem. Soc., 135 (2013) 9991-9994.
[35] Y. Kwon, S.C.S. Lai, P. Rodriguez, M.T.M. Koper, Electrocatalytic Oxidation of Alcohols on Gold in Alkaline Media: Base or Gold Catalysis?, J. Am. Chem. Soc., 133 (2011) 6914-6917.
[36] B.N. Zope, D.D. Hibbitts, M. Neurock, R.J. Davis, Reactivity of the Gold/Water Interface During Selective Oxidation Catalysis, Science, 330 (2010) 74-78.
[37] W.C. Ketchie, M. Murayama, R.J. Davis, Promotional effect of hydroxyl on the aqueous phase oxidation of carbon monoxide and glycerol over supported Au catalysts, Top. Catal., 44 (2007) 307-317.
[38] D. Basu, S. Basu, Synthesis, characterization and application of platinum based bi-metallic catalysts for direct glucose alkaline fuel cell, Electrochim. Acta, 56 (2011) 6106-6113.
[39] L.H.E. Yei, B. Beden, C. Lamy, Electrocatalytic oxidation of glucose at platinum in alkaline medium: on the role of temperature, J. Electroanal. Chem. Interf. Electrochem., 246 (1988) 349-362.
[40] K. Kleppe, The Effect of Hydrogen Peroxide on Glucose Oxidase from Aspergillus niger*, Biochem., 5 (1966) 139-143.
[41] L. Oliva, J.A. Fernandez-Lopez, X. Remesar, M. Alemany, The anomeric nature of glucose and its implications on its analyses and the influence of diet: are routine glycaemia measurements reliable enough?, J. Endocrinol. Metab., 9 (2019) 63-70.
[42] I. Miwa, K. Maeda, J. Okuda, Anomeric compositions of D-glucose in tissues and blood of rat, Experientia, 34 (1978) 167-169.
[43] C.M. Wong, K.H. Wong, X.D. Chen, Glucose oxidase: natural occurrence, function, properties and industrial applications, Appl. Microbiol. Biotechnol., 78 (2008) 927-938.
[44] D.P. Hickey, R.D. Milton, M. Rasmussen, S. Abdellaoui, K. Nguyen, S.D. Minteer, Fundamentals and applications of bioelectrocatalysis, Electrochemistry: Volume 13, The Royal Society of Chemistry2016, pp. 97-132.
[45] D. Siegmund, S. Metz, V. Peinecke, T.E. Warner, C. Cremers, A. Grevé, T. Smolinka, D. Segets, U.-P. Apfel, Crossing the Valley of Death: From Fundamental to Applied Research in Electrolysis, JACS Au, 1 (2021) 527-535.
[46] K. Ehelebe, N. Schmitt, G. Sievers, A.W. Jensen, A. Hrnjić, P. Collantes Jiménez, P. Kaiser, M. Geuß, Y.-P. Ku, P. Jovanovič, K.J.J. Mayrhofer, B. Etzold, N. Hodnik, M. Escudero-Escribano, M. Arenz, S. Cherevko, Benchmarking Fuel Cell Electrocatalysts Using Gas Diffusion Electrodes: Inter-lab Comparison and Best Practices, ACS Energy Lett., 7 (2022) 816-826.
[47] B.G. Pollet, S.S. Kocha, Using Ultrasound to Effectively Homogenise Catalyst Inks: Is this Approach Still Acceptable?, Johnson Matthey Technol. Rev., 66 (2022) 61-76.
[48] B.G. Pollet, Let's Not Ignore the Ultrasonic Effects on the Preparation of Fuel Cell Materials, Electrocatalysis, 5 (2014) 330-343.
[49] B.G. Pollet, J.T.E. Goh, The importance of ultrasonic parameters in the preparation of fuel cell catalyst inks, Electrochim. Acta, 128 (2014) 292-303.
[50] D. Higgins, C. Hahn, C. Xiang, T.F. Jaramillo, A.Z. Weber, Gas-Diffusion Electrodes for Carbon Dioxide Reduction: A New Paradigm, ACS Energy Lett., 4 (2018) 317-324.
[51] N.D. Nikolić, G. Branković, V.M. Maksimović, M.G. Pavlović, K.I. Popov, Application of pulsating overpotential regime on the formation of copper deposits in the range of hydrogen co-deposition, J. Solid State Electrochem., 14 (2010) 331-338.

[52] M. Ghaemi, L. Binder, Effects of direct and pulse current on electrodeposition of manganese dioxide, J. Power Sources, 111 (2002) 248-254.
[53] H. Jiang, Y. Sun, B. You, Dynamic Electrodeposition on Bubbles: An Effective Strategy toward Porous Electrocatalysts for Green Hydrogen Cycling, Acc. Chem. Res., 56 (2023) 1421-1432.
[54] L. Du, H. Xiong, H. Lu, L.-M. Yang, R.-Z. Liao, B.Y. Xia, B. You, Electroshock synthesis of a bifunctional nonprecious multi-element alloy for alkaline hydrogen oxidation and evolution, Exploration, 2 (2022) 20220024.
[55] P. Morandi, N. Tuleushova, S. Tingry, J. Cambedouzou, S.D. Minteer, D. Cornu, Y. Holade, Bromide-Regulated Anisotropic Growth of Desert-Rose-Like Nanostructured Gold onto Carbon Fiber Electrodes as Freestanding Electrocatalysts, ACS Appl. Energy Mater., 3 (2020) 7560-7571.
[56] Y. Holade, D.P. Hickey, S.D. Minteer, Halide-regulated growth of electrocatalytic metal nanoparticles directly onto a carbon paper electrode, J. Mater. Chem. A, 4 (2016) 17154-17162.
[57] A. Usher, D.C. McPhail, J. Brugger, A spectrophotometric study of aqueous Au(III) halide–hydroxide complexes at 25–80 °C, Geochim. Cosmochim. Acta, 73 (2009) 3359-3380.
[58] D.H. Evans, J.J. Lingane, Standard potentials of the couples involving $AuBr_4^-$, $AuBr_2^-$ and Au In bromide media, J. Electroanal. Chem., 6 (1963) 1-10.
[59] S.K. Chatterjee, X-ray Diffraction: Its Theory and Applications, 2nd ed., Prentice-Hall of India Pvt.Ltd, New Delhi, India, 2010.
[60] C. Suryanarayana, M.G. Norton, X-Ray Diffraction, A Pratical Approach, Plenum Publishing Corporation, New York, 1998, pp. 292.
[61] B.E. Warren, X-Ray Diffraction, 2 ed., Dover Publications, Inc., New York, 1990.
[62] M.F. Perutz, Sir Lawrence Bragg Nature, 233 (1971) 74-76.
[63] P. Rodriguez, Y. Kwon, M.T.M. Koper, The promoting effect of adsorbed carbon monoxide on the oxidation of alcohols on a gold catalyst, Nat. Chem., 4 (2012) 177-182.
[64] A.N. Kahyaoglu, Oxydation électrocatalytique du glycérol sur le platine, l'or et leurs alliages binaires, Thèse de Doctorat, Université de Poitiers, France1981.
[65] M.O. Finot, G.D. Braybrook, M.T. McDermott, Characterization of electrochemically deposited gold nanocrystals on glassy carbon electrodes, J. Electroanal. Chem., 466 (1999) 234-241.
[66] S. Hebié, Y. Holade, K. Maximova, M. Sentis, P. Delaporte, K.B. Kokoh, T.W. Napporn, A.V. Kabashin, Advanced Electrocatalysts on the Basis of Bare Au Nanomaterials for Biofuel Cell Applications, ACS Catal., 5 (2015) 6489-6496.
[67] Z. Wang, P. Liu, J. Han, C. Cheng, S. Ning, A. Hirata, T. Fujita, M. Chen, Engineering the internal surfaces of three-dimensional nanoporous catalysts by surfactant-modified dealloying, Nat. Commun., 8 (2017) 1066.
[68] A. Hamelin, Underpotential deposition of lead on single crystal faces of gold: Part I. The influence of crystallographic orientation of the substrate, J. Electroanal. Chem. Interf. Electrochem., 165 (1984) 167-180.
[69] N. Mayet, K. Servat, K.B. Kokoh, T.W. Napporn, Probing the Surface of Noble Metals Electrochemically by Underpotential Deposition of Transition Metals, Surfaces, 2 (2019) 257-276.
[70] F. Largeaud, K.B. Kokoh, B. Beden, C. Lamy, On the electrochemical reactivity of anomers: electrocatalytic oxidation of α- and β-d-glucose on platinum electrodes in acid and basic media, J. Electroanal. Chem., 397 (1995) 261-269.
[71] X. Liu, P. Cai, G. Wang, Z. Wen, Nickel doped MoS2 nanoparticles as precious-metal free bifunctional electrocatalysts for glucose assisted electrolytic H2 generation, Int. J. Hydrogen Energy, 45 (2020) 32940-32948.

[72] Y. Zhang, B. Zhou, Z. Wei, W. Zhou, D. Wang, J. Tian, T. Wang, S. Zhao, J. Liu, L. Tao, S. Wang, Coupling Glucose-Assisted Cu(I)/Cu(II) Redox with Electrochemical Hydrogen Production, Adv. Mater., 33 (2021) 2104791.
[73] Y. Xin, F. Wang, L. Chen, Y. Li, K. Shen, Superior bifunctional cobalt/nitrogen-codoped carbon nanosheet arrays on copper foam enable stable energy-saving hydrogen production accompanied with glucose upgrading, Green Chem., 24 (2022) 6544-6555.
[74] P. Du, J. Zhang, Y. Liu, M. Huang, Hydrogen generation from catalytic glucose oxidation by Fe-based electrocatalysts, Electrochem. Commun., 83 (2017) 11-15.
[75] C. Lin, P. Zhang, S. Wang, Q. Zhou, B. Na, H. Li, J. Tian, Y. Zhang, C. Deng, L. Meng, J. Wu, C. Liu, J. Hu, L. Zhang, Engineered porous Co–Ni alloy on carbon cloth as an efficient bifunctional electrocatalyst for glucose electrolysis in alkaline environment, J. Alloys Compd., 823 (2020) 153784.
[76] D. Zheng, J. Li, S. Ci, P. Cai, Y. Ding, M. Zhang, Z. Wen, Three-birds-with-one-stone electrolysis for energy-efficiency production of gluconate and hydrogen, Appl. Catal. B: Env., 277 (2020) 119178.
[77] H. Zhou, Y. Ren, B. Yao, Z. Li, M. Xu, L. Ma, X. Kong, L. Zheng, M. Shao, H. Duan, Scalable electrosynthesis of commodity chemicals from biomass by suppressing non-Faradaic transformations, Nat. Commun., 14 (2023) 5621.
[78] Y. Wang, W. Yan, M. Ni, C. Zhu, H. Du, Surface valence regulation of cobalt–nickel foams for glucose oxidation-assisted water electrolysis, Chem. Commun., 59 (2023) 2485-2488.
[79] A. Lasia, Electrochemical Impedance Spectroscopy and its Applications, Springer-Verlag, New York, NY, USA, 2014.
[80] M.E. Orazem, B. Tribollet, Electrochemical Impedance Spectroscopy, 2 ed., John Wiley & Sons, Inc. , Hoboken, New Jersey, USA, 2017.
[81] M. Xu, L. Zhang, F. Zhao, One-Pot Aqueous Synthesis of Icosahedral Au as Bifunctional Candidates for Enhanced Glucose Electrooxidation and Surface-Enhanced Raman Scattering, ACS Appl. Mater. Interfaces., 12 (2020) 12186-12194.
[82] K. Torigoe, M. Takahashi, K. Tsuchiya, K. Iwabata, T. Ichihashi, K. Sakaguchi, F. Sugawara, M. Abe, High-Power Abiotic Direct Glucose Fuel Cell Using a Gold–Platinum Bimetallic Anode Catalyst, ACS Omega, 3 (2018) 18323-18333.
[83] C. Lemoine, L. Dubois, T.W. Napporn, K. Servat, K.B. Kokoh, Electrochemical Energy Conversion from Direct Oxidation of Glucose on Active Electrode Materials, Electrocatalysis, 11 (2020) 170-179.
[84] J. Wang, F. Chen, Y. Jin, Y. Lei, Dilute Au-Containing Ag Nanosponges as a Highly Active and Durable Electrocatalyst for Oxygen Reduction and Alcohol Oxidation Reactions, ACS Appl. Mater. Interfaces., 10 (2018) 6276-6287.
[85] M. Xu, Y. Sui, G. Xiao, X. Yang, Y. Wei, B. Zou, Kinetically controlled synthesis of nanoporous Au and its enhanced electrocatalytic activity for glucose-based biofuel cells, Nanoscale, 9 (2017) 2514-2520.
[86] A.J. Bard, L.R. Faulkner, Electrochemical Methods: Fundamentals and Applications, 2nd ed., John Wiley & Sons, Inc., USA, 2001.
[87] R. Guidelli, R.G. Compton, J.M. Feliu, E. Gileadi, J. Lipkowski, W. Schmickler, S. Trasatti, Defining the transfer coefficient in electrochemistry: An assessment (IUPAC Technical Report), Pure Appl. Chem., 86 (2014) 245-258.
[88] E. Laborda, M.C. Henstridge, R.G. Compton, Asymmetric Marcus theory: Application to electrode kinetics, J. Electroanal. Chem., 667 (2012) 48-53.
[89] M. Chatenet, J. Benziger, M. Inaba, S. Kjelstrup, T. Zawodzinski, R. Raccichini, Good practice guide for papers on fuel cells and electrolysis cells for the Journal of Power Sources, J. Power Sources, 451 (2020) 227635.

[90] A.J. Bard, L.R. Faulkner, H.S. White, Electrochemical Methods: Fundamentals and Applications, 3rd ed., John Wiley & Sons, Inc., USA, 2022.
[91] K. Elsøe, L. Grahl-Madsen, G.G. Scherer, J. Hjelm, M.B. Mogensen, Electrochemical Characterization of a PEMEC Using Impedance Spectroscopy, J. Electrochem. Soc., 164 (2017) F1419.
[92] P. Lettenmeier, R. Wang, R. Abouatallah, S. Helmly, T. Morawietz, R. Hiesgen, S. Kolb, F. Burggraf, J. Kallo, A.S. Gago, K.A. Friedrich, Durable Membrane Electrode Assemblies for Proton Exchange Membrane Electrolyzer Systems Operating at High Current Densities, Electrochim. Acta, 210 (2016) 502-511.
[93] S. Sun, Z. Shao, H. Yu, G. Li, B. Yi, Investigations on degradation of the long-term proton exchange membrane water electrolysis stack, J. Power Sources, 267 (2014) 515-520.
[94] C. Rozain, P. Millet, Electrochemical characterization of Polymer Electrolyte Membrane Water Electrolysis Cells, Electrochim. Acta, 131 (2014) 160-167.

Figure and Table captions

Fig. 1. a) Chair conformations of the predominant forms of glucose in aqueous solution under ambient conditions of temperature and pressure: pyranose forms account for 99% (vide infra). b) Thermodynamic E-pH diagrams for water and "glucose" (simplified as RCHO albeit cyclic), assuming electrooxidation of the anomeric carbon in a 2-electron pathway, adapted from refs. [16,17].

Fig. 2. Physical characterization. a) Galvanostatic electroshock grow of Au or Pt particles onto the GDE (parameters: $\tau_{ON} = \tau_{OFF} = 5$ s, $I_{ON} = -2.7$ mA, $I_{OFF} = 0$ μA, $N_{cycles} = 180$, GDE size = 3 cm × 3 cm (one side masked), electrolyte = 0.1 M KNO_3 + 2.6 mM KBr, temperature = 25 °C, gentle stirring, $C_{precursor} = 0.22$ mM ($HAuCl_4 \cdot 3H_2O$ or $H_2PtCl_6 \cdot 6H_2O$). b) Overview SEM image of typical GDE-Au electrode after electrodeposition. c) XRD patterns of the blank and as-synthesized electrodes (top), and references (bottom). d) EDX spectra as-synthesized electrodes. Backscattered SEM images and EDX maps of: e) GDE-Au, and f) GDE-Pt.

Fig. 3. Representative SEM images, at different magnifications, of the as-synthesized: a1-a4) GDE-Pt, and b1-b8) GDE-Au.

Fig. 4. Electrochemical characterization. a) CVs (50 mV s^{-1}, 1 M KOH, 25 °C) of bare GDE and synthesized GDE-Pt and GDE-Au. b) CVs (1 M KOH + 1 mM $Pb(NO_3)_2$) of GDE-Au for Pb_{UPD} at different scan rates. c) LSVs (5 mV s^{-1}, 1 M KOH, 25 °C) of HER of synthesized GDE-Pt and commercial Pt/C loaded onto GDE at the same metal content (33 μg_{Pt} cm^{-2}). d,e) Background current corrected voltammograms (50 mV s^{-1}, 1 M KOH, 0.1 M glucose, 25 °C) of synthesized GDE-Au and commercial Au/C loaded onto GDE at the same metal content (82 μg_{Au} cm^{-2}) for D-, α-D-, and β-D-glucose: d) Current per estimated geometric surface area, and e) Current per layer of fibers of GDE substrate containing catalytic particles. f) R_{ct}-based Tafel plots from EIS (1 M KOH, 0.1 M glucose, 25 °C) of GDE-Au for D-, α-D-, and β-D-glucose. g-i) Complex-plane Nyquist impedance plots recorded at different electrode potentials (1 M

KOH, 0.1 M glucose, 25 °C) of GDE-Au for: g) D-, h) α-D-, and i) β-D-glucose; inset is the EEC of R_{Ω} + Q_{CPE}//R_{ct}.

Fig. 5. Electrolyzer performance (25 °C): effect of glucose concentration. a) Scheme of the electrolysis cell. b) Complex-plane Nyquist impedance plots recorded at different cell voltages in the absence of glucose: inset is the EEC of R_{Ω}+$Q_{CPE\text{-}a}$//$R_{ct\text{-}a}$+$Q_{CPE\text{-}c}$//$R_{ct\text{-}c}$. c) Complex-plane Nyquist impedance plots recorded at different cell voltages in the presence of different concentrations of D-glucose: inset is the EEC of R_{Ω}+$Q_{CPE\text{-}a}$//$R_{ct\text{-}a}$+$Q_{CPE\text{-}c}$//$R_{ct\text{-}c}$. d,e) Polarization curves for different concentrations of D-glucose: d) Potentiostatic method (step of 0.05 V), and e) LSV method (scan rate of 0.05 V s^{-1}). Cathode: 1 M KOH (150 mL min^{-1}, 25 °C) and GDE-Pt (33 μg_{Pt} cm^{-2}). Anode: 1 M KOH + 0.1 M D-glucose (100 mL min^{-1}, 25 °C) and GDE-Au (82 μg_{Pt} cm^{-2}). Hydroxide anion exchange membrane: Sustainion® X37-50 grade RT (5 cm^2). Error bars represent one standard deviation (n = 3).

Fig. 6. Electrolyzer performance (25 °C): effect of the nature of glucose substrate. a,b) Polarization curves for different type of glucose (D-, α-D-, and β-D-glucose): a) Potentiostatic method (step of 0.05 V), and b) LSV method (scan rate of 0.05 V s^{-1}). c) Complex-plane Nyquist impedance plots recorded at 0.6 V in the presence of different type of glucose (D-, α-D-, and β-D-glucose): inset is the EEC of R_{Ω}+$Q_{CPE\text{-}a}$//$R_{ct\text{-}a}$+$Q_{CPE\text{-}c}$//$R_{ct\text{-}c}$. d-g) Post-mortem SEM images of the electrodes after electrolysis: d-f) GDE-Au, and g) GDE-Pt. Cathode: 1 M KOH (150 mL min^{-1}, 25 °C) and GDE-Pt (33 μg_{Pt} cm^{-2}). Anode: 1 M KOH + 0.1 M D-glucose (100 mL min^{-1}, 25 °C) and GDE-Au (82 μg_{Pt} cm^{-2}). Hydroxide anion exchange membrane: Sustainion® X37-50 grade RT (5 cm^2). Error bars represent one standard deviation (n = 3).

Table 1. Quantitative data from ICP-OES and XRD.

Entry	ICP-OES[a]		XRD	
	Metal content [wt%]	Loading (single face) [μg_{metal} cm^{-2}]	Lattice parameter [Å]	Crystallite size [nm]
GDE-Au	0.886	82	4.07	56
GDE-Pt	0.360	33	3.90	12

[a]%RSD (relative standard deviation) = 0.28 and 0.52 for GDE-Au and GDE-Pt, respectively.

Table 2. Fitted EIS data of glucose oxidation by R_Ω+Q_{CPE}//R_{ct} (1 M KOH, 25 °C).

Entry	$E_{applied}$ [V vs RHE]	R_Ω [Ω cm^2]	R_{ct} [Ω cm^2]	Q_{CPE} [mF cm^2 $s^{(a-1)}$]	a
D-glucose	0.35	2.3	45.6	0.2	0.9
	0.37	2.3	31.2	0.2	0.9
	0.40	2.3	15.2	0.3	0.8
	0.45	2.2	8.9	0.3	0.8
α-D-glucose	0.35	2.3	56.3	0.2	0.9
	0.37	2.3	35.9	0.2	0.9
	0.40	2.3	14.3	0.2	0.9
	0.45	2.3	9.6	0.2	0.8
β-D-glucose	0.35	2.2	54.4	0.3	0.9
	0.37	2.2	35.2	0.3	0.9
	0.40	2.2	15.8	0.3	0.9
	0.45	2.2	9.7	0.3	0.8

Table 3. Fitted EIS data of the electrolysis cell by R_Ω+$Q_{CPE\text{-}a}$//$R_{ct\text{-}a}$+$Q_{CPE\text{-}c}$//$R_{ct\text{-}c}$ (25 °C): effect of glucose concentration. Catholyte: 1 M KOH (150 mL min^{-1}, 25 °C). Anolyte: 1 M KOH + 0.1 M D-glucose (100 mL min^{-1}, 25 °C). Hydroxide anion exchange membrane: Sustainion® X37-50 grade RT (5 cm^2).

D-glucose (M)	$U_{applied}$ [V]	R_Ω [Ω cm^2]	Anode			Cathode		
			$R_{ct\text{-}a}$ [Ω cm^2]	$Q_{CPE\text{-}a}$ [mF cm^2 $s^{(a-1)}$]	a	$R_{ct\text{-}c}$ [Ω cm^2]	$Q_{CPE\text{-}c}$ [mF cm^2 $s^{(a-1)}$]	a
0	1.5	0.20	3.86	46.4	0.84	0.50	6.5	0.97
0.1	0.6	0.19	23.77	50.9	0.82	1.00	18.7	0.87
0.5	0.6	0.23	8.09	58.8	0.76	0.85	19.0	0.89

Table 4. Fitted EIS data of the electrolysis by R_{Ω}+$Q_{CPE\text{-}a}$//$R_{ct\text{-}a}$+$Q_{CPE\text{-}c}$//$R_{ct\text{-}c}$: effect of the type of glucose. Catholyte: 1 M KOH (150 mL min^{-1}, 25 °C). Anolyte: 1 M KOH + 0.1 M glucose (100 mL min^{-1}, 25 °C). Hydroxide anion exchange membrane: Sustainion® X37-50 grade RT (5 cm^2).

Entry	$U_{applied}$ [V]	R_{Ω} [Ω cm^2]	Anode			Cathode		
			$R_{ct\text{-}a}$ [Ω cm^2]	$Q_{CPE\text{-}a}$ [mF cm^2 $s^{(a-1)}$]	a	$R_{ct\text{-}c}$ [Ω cm^2]	$Q_{CPE\text{-}c}$ [mF cm^2 $s^{(a-1)}$]	a
D-glucose	0.6	0.19	23.77	50.9	0.82	1.00	13.7	0.87
α-D-glucose	0.6	0.17	12.43	49.3	0.83	0.90	13.1	0.93
β-D-glucose	0.6	0.20	29.32	46.4	0.85	1.10	14.7	0.90

Table 5. Performance of relevant data from literature towards glucose electrolysis in alkaline electrolyte. Empty box (–) means that the original article does not provide such data. GDE: gas diffusion electrode; CC: conductive carbon cloth; AEM: hydroxide anion exchange membrane

Cathode		Separator (temperature)	Anode		Performance	Ref.
Electrocatalyst (loading)	Catholyte		Electrocatalyst (loading)	Anolyte		
GDE-Pt (0.03 mg cm^{-2})	1 M KOH	AEM (25 °C)	GDE-Au (0.08 mg cm^{-2})	1 M KOH + 0.1 M D-glucose	• OCV: 0.1 V • Cell voltage V at 10 mA cm^{-2}: 0.54 V • Current density at 0.5 V: 5.0 ± 1.2 mA cm^{-2}; • Current density at 1 V: 44.3 ± 8.8 mA cm^{-2}; • Selectivity in glucose oxidation: 100% in gluconate	Herein
				1 M KOH + 0.1 M α-D-glucose	• OCV: 0.1 V • Cell voltage V at 10 mA cm^{-2}: 0.52 V • Current density at 0.5 V: 7.8 ± 1.8 mA cm^{-2}; • Current density at 1 V: 85.6 ± 17.1 mA cm^{-2}; • Selectivity in glucose oxidation: 100% in gluconate	

				1 M KOH + 0.1 M β-D-glucose	• OCV: 0.1 V • Cell voltage V at 10 mA cm^{-2}: 0.54 V • Current density at 0.5 V: 6.0 ± 0.8 mA cm^{-2}; • Current density at 1 V: 30.5 ± 0.8 mA cm^{-2}; • Selectivity in glucose oxidation: 100% in gluconate	
				1 M KOH + 0.5 M D-glucose	• OCV: 0.1 V • Cell voltage V at 10 mA cm^{-2}: 0.47 V • Current density at 0.5 V: 11.0 ± 0.2 mA cm^{-2}; • Current density at 1 V: 102.9 ± 4.9 mA cm^{-2}; • Selectivity in glucose oxidation: 100% in gluconate	
$Fe_{0.1}$-$CoSe_2$/CC. (4.93 mg cm^{-2})	0.5 M H_2SO_4	Bipolar membrane	$Fe_{0.1}$-$CoSe_2$/CC. (4.93 mg cm^{-2})	1 M KOH	• OCV: 0.4 V • Cell voltage V at 10 mA cm^{-2}: 0.72 V • Current density at 1 V: 30 mA cm^{-2}; • Selectivity in glucose oxidation: 87% in gluconate	Appl. Catal. B: Env., 277 (2020) 119178. [76]
Nickel foam	1 M KOH	No separator	CoOOH/ nickel foam	1 M KOH + 0.15 M	• Cell voltage ~2.1 V at 50 mA cm^{-2} • Cell voltage ~2.3 V at 100 mA cm^{-2} • Cell voltage ~2.73 V at 166.7 mA cm^{-2} • Selectivity in glucose oxidation: 67% in formate	Nat. Commun., 14 (2023) 5621. [77]
Pt/C (0.5 mg cm^{-2})	0.1 M NaOH + 0.1 M glucose	Blotting paper	Pd_3Au_7/C (0.5 mg cm^{-2})	0.1 M NaOH + 0.1 M glucose	• Current at cell voltage of 0.4 V: 37 mA for 25 cm^2 (1.5 mA cm^{-2}) • Selectivity in glucose oxidation: 91-98% in gluconate	Appl. Catal. B: Env., 243 (2019) 641-656. [25]
Cobalt-nickel foam	1 M KOH	AEM	Cobalt-nickel foam	1 M KOH + 0.15 M D-glucose	• OCV: 1.5 V • Cell voltage V at 10 mA cm^{-2}: 2.0 V (1.65 after iR-drop correction) • Selectivity in glucose oxidation: glucarate	Chem. Commun., 59 (2023) 2485-2488. [78]
Ni-MoS_2	1 M KOH	AEM (RT)	Ni-MoS_2	1 M KOH + 0.3 M glucose	• OCV: 1.1 V • Cell voltage V at 10 mA cm^{-2}: 1.67 V	Hydrogen Energy, 45 (2020)

					• Cell voltage V at 100 mA cm^{-2}: 1.9 V	32940-32948. [71]
Nanostructured NiFe nitride ($NiFeN_x$) onto Ni foams	1 M KOH	AEM	Nanostructured NiFe oxide (NiFeOx) onto Ni foams	1 M KOH + 0.5 M glucose	• OCV: 1.2 V • Cell voltage V at 10 mA cm^{-2}: 1.24 V • Cell voltage V at 100 mA cm^{-2}: 1.29 V • Selectivity in glucose oxidation: 87% glucarate	Nat. Commun., 11 (2020) 265. [21]
Pt/C	1 M KOH	AEM	$Cu(OH)_2$/copper foam	1 M KOH + 0.1 M glucose	• OCV: 0.6 V • Cell voltage V at 10 mA cm^{-2}: 0.74 V • Cell voltage V at 50 mA cm^{-2}: 0.83 V • Cell voltage V at 100 mA cm^{-2}: 0.9 V • Selectivity in glucose oxidation: gluconate	Adv. Mater., 33 (2021) 2104791. [72]
Cobalt/nitrogen-co-doped carbon (CoNC) nanosheet arrays on copper foam	1 M KOH + 0.1 M glucose	No separator	Cobalt/nitrogen-co-doped carbon (CoNC) nanosheet arrays on copper foam	1 M KOH + 0.1 M glucose	• OCV: 0.6 V • Cell voltage V at 10 mA cm^{-2}: 0.66 V • Cell voltage V at 50 mA cm^{-2}: 0.82 V • Cell voltage V at 100 mA cm^{-2}: 0.90 V • Selectivity in glucose oxidation: gluconate + glucarate	Green Chem., 24 (2022) 6544-6555. [73]
Pt/C (1.5 mg cm^{-2})	10 M KOH	No separator	Iron phosphide films (Fe_2P) grown in situ on stainless steel mesh (SSM)	10 M KOH + 0.5 M glucose	• OCV: 1.1 V • Cell voltage V at 10 mA cm^{-2}: 1.22 V • Cell voltage V at 50 mA cm^{-2}: 1.50 V • Cell voltage V at 100 mA cm^{-2}: 1.55 V	Electrochem. Commun., 83 (2017) 11-15. [74]
Co-Ni alloy on carbon cloth ($Co_{0.5}Ni_{0.5}$/CC)	1 M KOH	No separator	Co-Ni alloy on carbon cloth ($Co_{0.5}Ni_{0.5}$/CC)	1 M KOH + 0.1 M glucose	• OCV: 1.2 V • Cell voltage V at 10 mA cm^{-2}: 1.39 V • Cell voltage V at 50 mA cm^{-2}: 1.52 V • Cell voltage V at 100 mA cm^{-2}: 1.60 V	J. Alloys Compd., 823 (2020) 153784. [75]

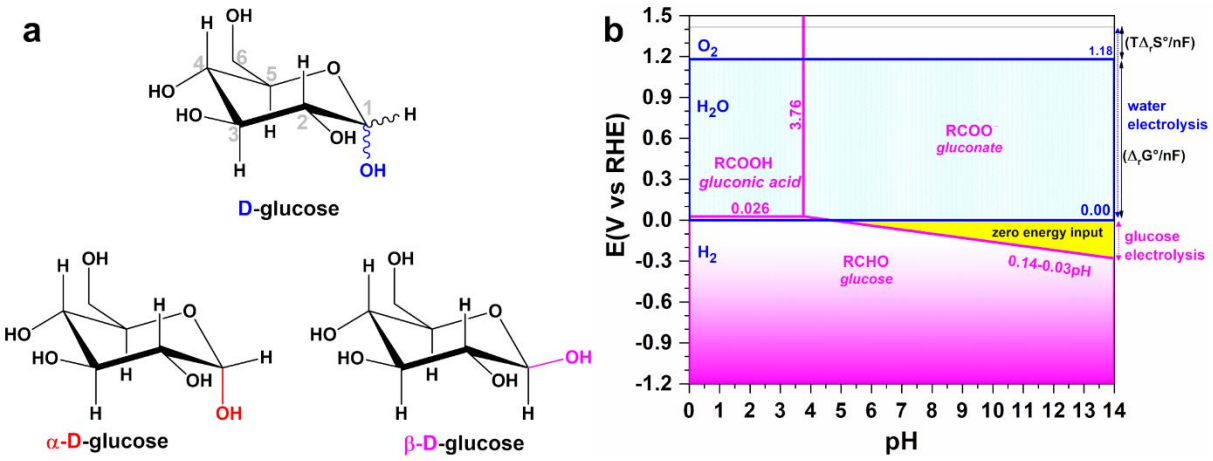
a
D-glucose
α-D-glucose
β-D-glucose
b
E(V vs RHE)
pH
O2
H2O
H2
RCOOH
gluconic acid
RCOO
gluconate
RCHO
glucose
3.76
0.026
1.18
0.00
0.14-0.03pH
zero energy input
water electrolysis
glucose electrolysis
(TΔrS°/nF)
(ΔrG°/nF)

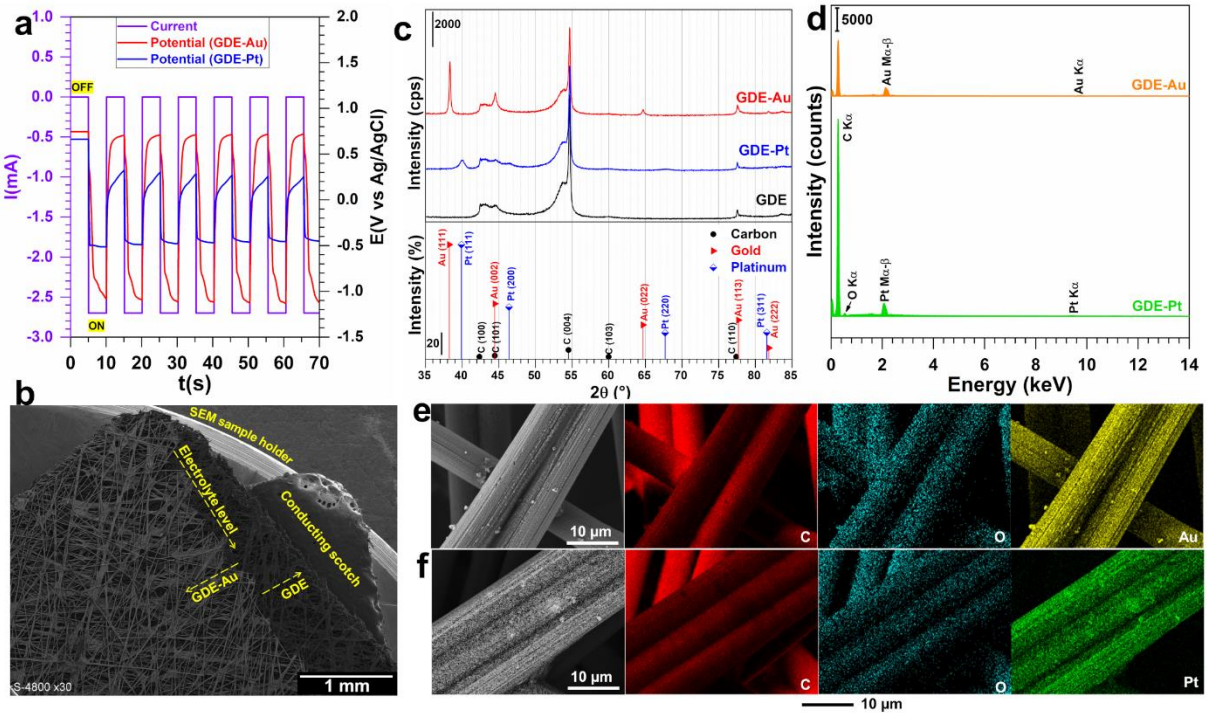
a
Current
Potential (GDE-Au)
Potential (GDE-Pt)
OFF
ON
I(mA)
E(V vs Ag/AgCl)
t(s)
c
2000
GDE-Au
GDE-Pt
GDE
Intensity (cps)
Intensity (%)
Carbon
Gold
Platinum
2θ (°)
d
5000
Au Mα-β
Au Kα
C Kα
O Kα
Pt Mα-β
Pt Kα
GDE-Au
GDE-Pt
Intensity (counts)
Energy (keV)
b
SEM sample holder
Electrolyte level
Conducting scotch
GDE-Au
GDE
S-4800 x30
1 mm
e
10 µm
C
O
Au
f
10 µm
C
O
Pt
10 µm

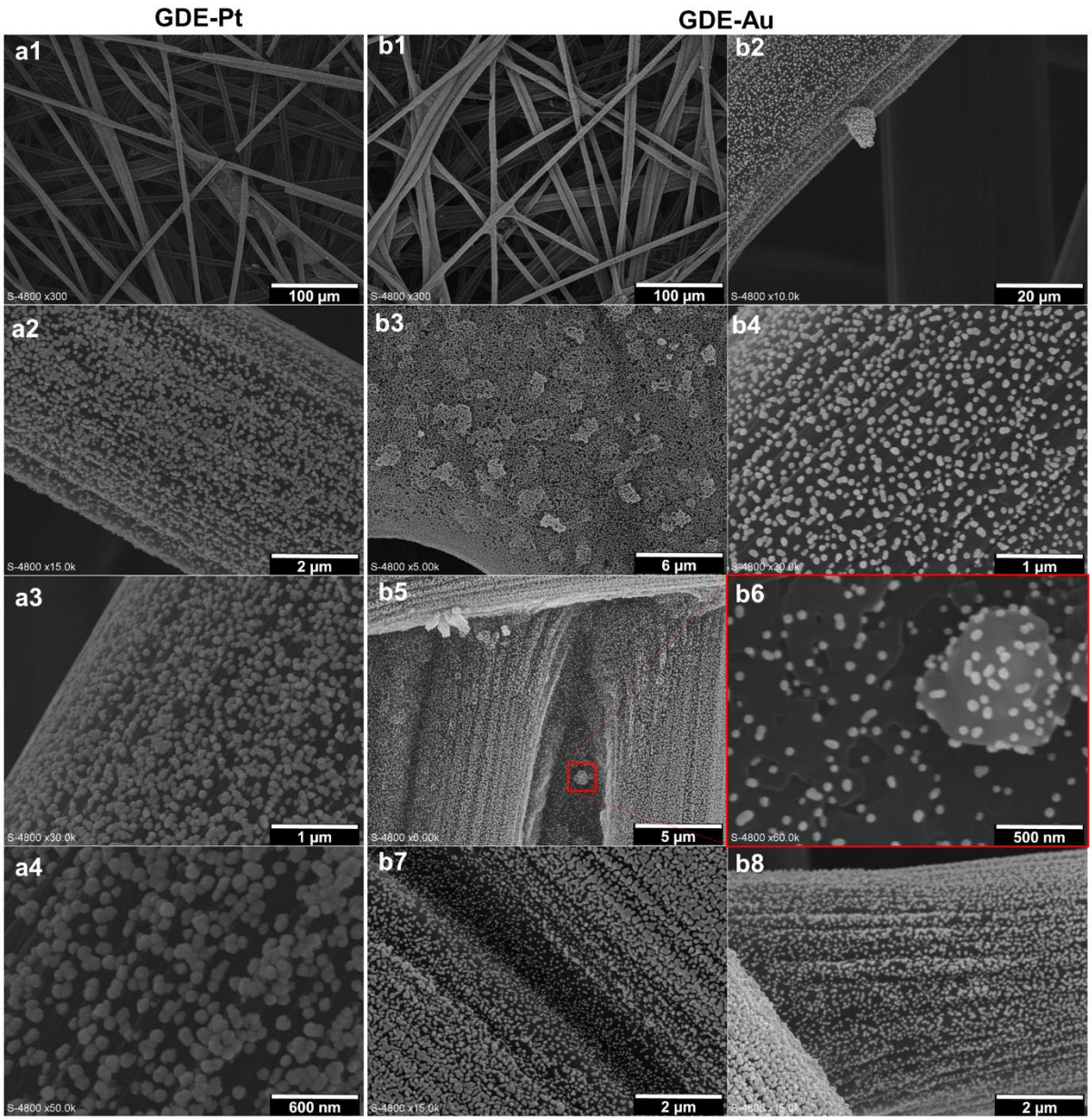
GDE-Pt
GDE-Au
a1
S-4800 x300
100 µm
b1
S-4800 x300
100 µm
b2
S-4800 x10.0k
20 µm
a2
S-4800 x15.0k
2 µm
b3
S-4800 x5.00k
6 µm
b4
S-4800 x30.0k
1 µm
a3
S-4800 x30.0k
1 µm
b5
S-4800 x6.00k
5 µm
b6
S-4800 x60.0k
500 nm
a4
S-4800 x50.0k
600 nm
b7
S-4800 x15.0k
2 µm
b8
2 µm

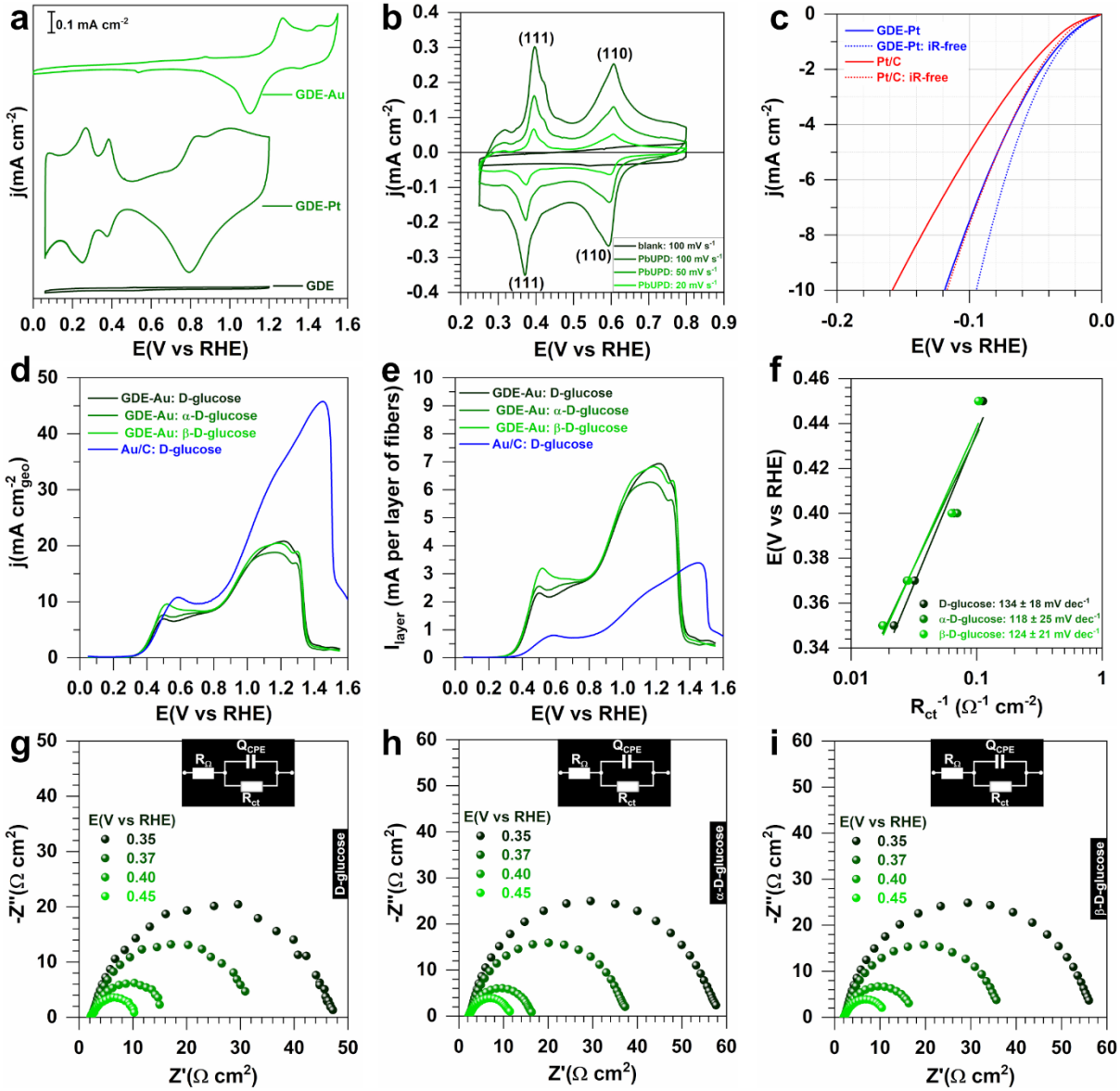
a
0.1 mA cm-2
GDE-Au
GDE-Pt
GDE
j(mA cm-2)
E(V vs RHE)
b
(111)
(110)
(110)
(111)
blank: 100 mV s-1
PbUPD: 100 mV s-1
PbUPD: 50 mV s-1
PbUPD: 20 mV s-1
j(mA cm-2)
E(V vs RHE)
c
GDE-Pt
GDE-Pt: iR-free
Pt/C
Pt/C: iR-free
j(mA cm-2)
E(V vs RHE)
d
GDE-Au: D-glucose
GDE-Au: α-D-glucose
GDE-Au: β-D-glucose
Au/C: D-glucose
j(mA cm-2geo)
E(V vs RHE)
e
GDE-Au: D-glucose
GDE-Au: α-D-glucose
GDE-Au: β-D-glucose
Au/C: D-glucose
Ilayer (mA per layer of fibers)
E(V vs RHE)
f
D-glucose: 134 ± 18 mV dec-1
α-D-glucose: 118 ± 25 mV dec-1
β-D-glucose: 124 ± 21 mV dec-1
E(V vs RHE)
Rct-1 (Ω-1 cm-2)
g
RΩ
QCPE
Rct
E(V vs RHE)
0.35
0.37
0.40
0.45
D-glucose
-Z''(Ω cm2)
Z'(Ω cm2)
h
RΩ
QCPE
Rct
E(V vs RHE)
0.35
0.37
0.40
0.45
α-D-glucose
-Z''(Ω cm2)
Z'(Ω cm2)
i
RΩ
QCPE
Rct
E(V vs RHE)
0.35
0.37
0.40
0.45
β-D-glucose
-Z''(Ω cm2)
Z'(Ω cm2)

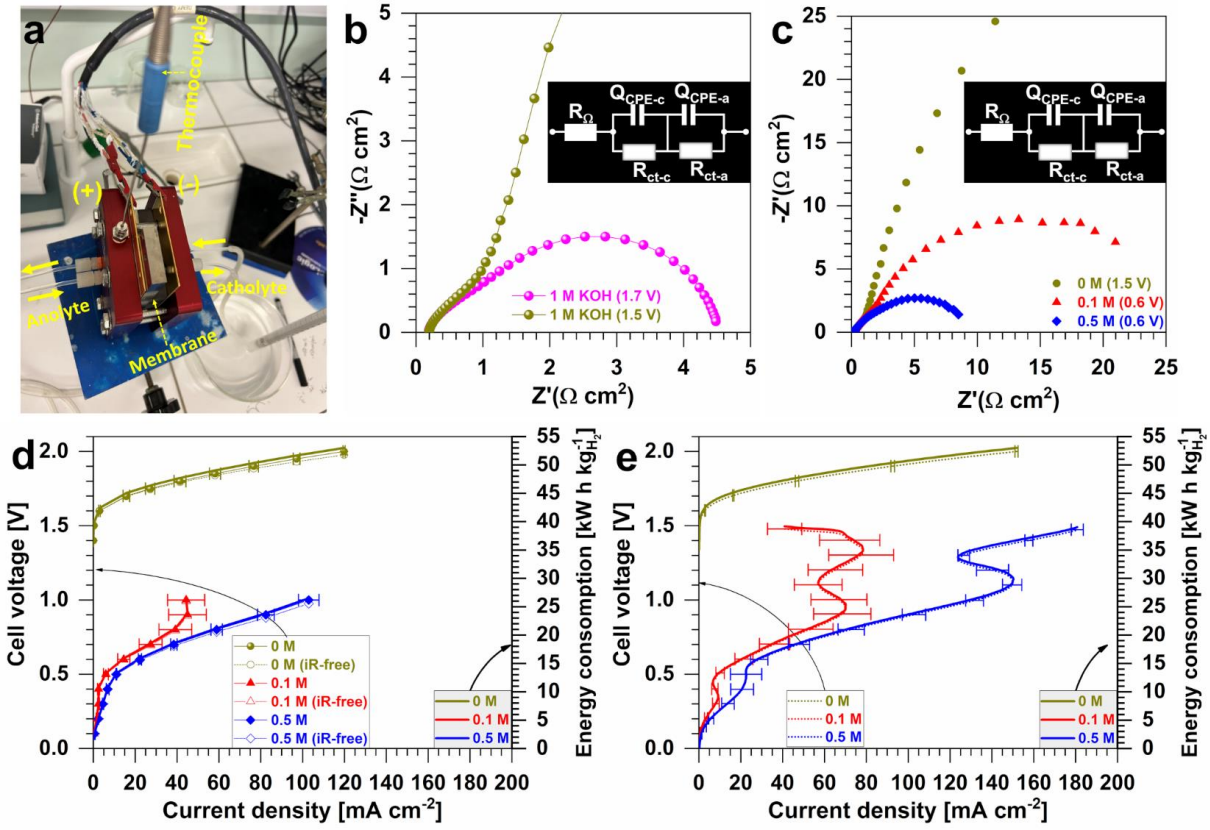
a
Thermocouple
(+)
(-)
Catholyte
Anolyte
Membrane
b
-Z''(Ω cm²)
Z'(Ω cm²)
1 M KOH (1.7 V)
1 M KOH (1.5 V)
c
-Z'(Ω cm²)
Z'(Ω cm²)
0 M (1.5 V)
0.1 M (0.6 V)
0.5 M (0.6 V)
d
Cell voltage [V]
Energy consomption [kW h kg⁻¹H₂]
Current density [mA cm⁻²]
0 M
0 M (iR-free)
0.1 M
0.1 M (iR-free)
0.5 M
0.5 M (iR-free)
e
Cell voltage [V]
Energy consomption [kW h kg⁻¹H₂]
Current density [mA cm⁻²]
0 M
0.1 M
0.5 M

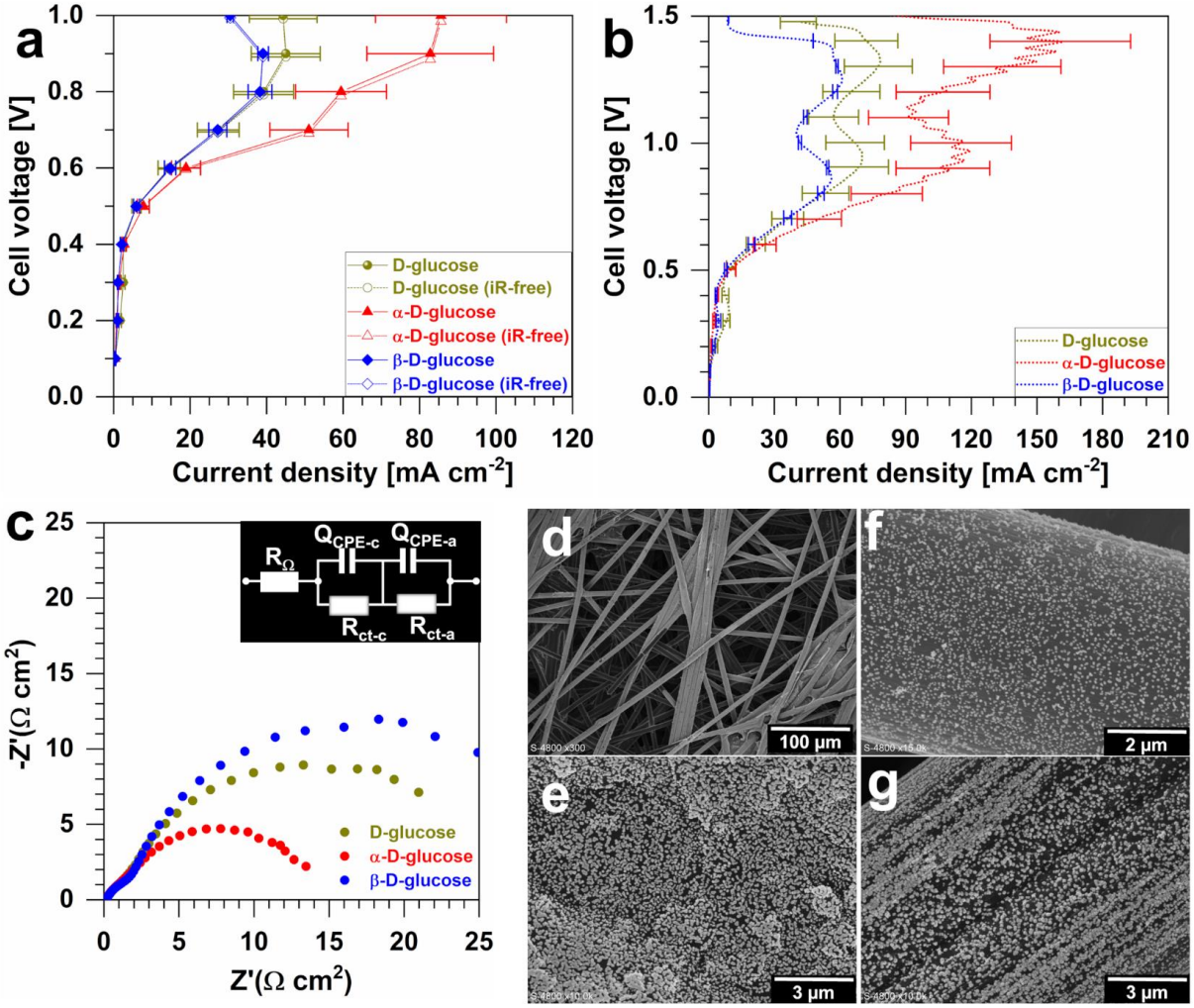
a
Cell voltage [V]
Current density [mA cm-2]
D-glucose
D-glucose (iR-free)
α-D-glucose
α-D-glucose (iR-free)
β-D-glucose
β-D-glucose (iR-free)
b
Cell voltage [V]
Current density [mA cm-2]
D-glucose
α-D-glucose
β-D-glucose
c
-Z'(Ω cm2)
Z'(Ω cm2)
RΩ
QCPE-c
QCPE-a
Rct-c
Rct-a
D-glucose
α-D-glucose
β-D-glucose
d
100 µm
f
2 µm
e
3 µm
g
3 µm